Dynamic Membranes

DOI: 10.1002/anie.201201686

Dynamic Interactive Membranes with Pressure-Driven Tunable Porosity and Self-Healing Ability**

Prashant Tyagi, André Deratani, Denis Bouyer, Didier Cot, Valérie Gence, Mihail Barboiu, Trang N. T. Phan, Denis Bertin, Didier Gigmes, and Damien Quemener**

Scientific interest in dynamic interactive systems with engineered interactions on extended scales is continuously growing because these systems may display novel properties not present at the molecular level.[1–3] Understanding and controlling the scale-up from the molecular level toward nanoscale dimensions[4–6] might provide new insights into basic features in the design of emergent systems at the heart of modern technologies such as tissue engineering,[7] artificial organs,[8] catalysis,[9] membrane filtration,[10] and sensing.[11] The de novo design of porous systems used as mechanical supports, molecular capacitors/distributors, or gating effectors and the use of strategies based on self-healing,[12–14] self-cleaning,[15,16] and stimuli-response[17] properties has become an area of growing interest. Classical membranes for water filtration are subjected to strong compression depending on their structural behavior and bulk porosity.[18,19] Irreversible compaction is usually effected in order to reach a steady-state flux, giving the membrane a stable pore size. In contrast, a responsive membrane can self-regulate its performance according to changes in environmental conditions such as pH, temperature, light, and ionic strength.[20–22] In the present work, the ABA triblock copolymer poly(styrene-*co*-acrylonitrile)-*b*-poly(ethylene oxide)-*b*-poly(styrene-*co*-acrylonitrile) (PSAN-*b*-PEO-*b*-PSAN) has been used to generate flower-like micelles. They consist of a compressible hydrophilic soft corona of PEO (26 vol%) and a hydrophobic hard core of PSAN which maintains the micelle's structural integrity (Figure 1). When a copolymer solution is spin-coated onto a silicon wafer, evaporation of the solvent results in the formation of a porous film through the assembly of micelles 50 nm in diameter. Reversible noncovalent interactions between the micelles mediate their dynamic self-assembly at the macroscopic level such that there is free volume between the micelles, imparting nanoporosity to the film.[23–27]

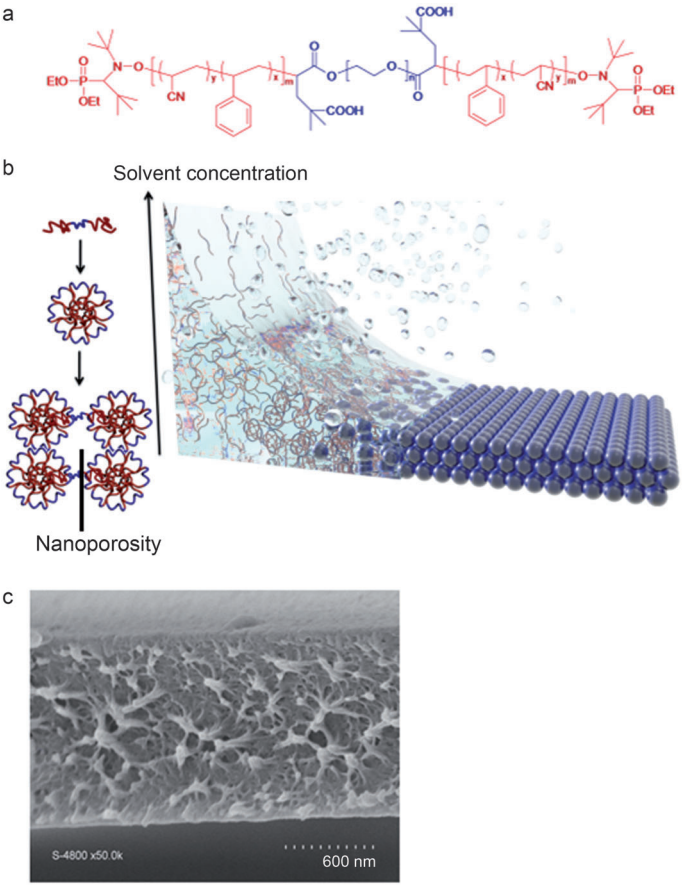

Figure 1. Three-dimensional self-assembled membrane film: a) Chemical structure of the ABA triblock copolymer. b) Sketch of the membrane formation: during the course of the solvent evaporation, the increase of the block copolymer concentration triggers their self-assembly into micelles, which assemble in three dimensions forming a dynamic interactive membrane film. c) Scanning electron microscopy (SEM) image of the film.

In addition to the reversible interactions of the PEO chains, the micelle assembly is also partially reinforced by bridging links between the ABA copolymer and the A blocks of two different micelle cores (Figure 1 b and Figures S1–S4 in the Supporting Information).[28,29] The morphology of these micellar systems can be fine-tuned for different functions. Evidence for morphological changes was obtained in studies of water permeation in which the water pressure orthogonal to the membrane surface was varied. For relative water pressures from 0.04 to 3 bar, the water flow resistance *R* of the

[*] P. Tyagi, Dr. A. Deratani, Dr. D. Bouyer, D. Cot, V. Gence, Dr. M. Barboiu, Dr. D. Quemener
Institut Européen des Membranes, UMR 5635 (CNRS-ENSCM-UM2)
Place E. Bataillon CC047, 34095 Montpellier (France)
E-mail: mihai.barboiu@iemm.univ-montp2.fr
damien.quemener@iemm.univ-montp2.fr
Dr. T. N. T. Phan, Prof. D. Bertin, Dr. D. Gigmes
Laboratoire Chimie Provence, Chimie Radicalaire, Organique et Polymères de Spécialité, Université d'Aix Marseille (France)

[**] This work was supported by a grant from the French National Agency for Research (ANR-07-NANO-055) and by a starting grant for young researchers from the University of Montpellier 2 (Scientific council). We thank M. Bonniol for his technical assistance and M. Ramonda for the AFM.

Supporting information for this article is available on the WWW under http://dx.doi.org/10.1002/anie.201201686.

WILEY ONLINE LIBRARY
© 2012 Wiley-VCH Verlag GmbH & Co. KGaA, Weinheim

material increased (Figure 2a,b and Figure S5 in the Supporting Information), while the porosity ε decreased from 35% to 5%. The pressure induces the decrease of the interstitial volume by compression of micelle's soft corona.

Between pressures of 2 and 3 bar, the compression is at its maximum and a plateau for R and ε is observed. Beyond 3 bar, the water flow resistance decreases dramatically and the porosity change is found to be irreversible. Atomic force microscopy (AFM) images revealed that when the self-assembled membrane film is subjected to water flow, the spherical particles rearrange into a more compact ordering (Figure 2c and Figure S6 and Table S1 in the Supporting Information). Up to a pressure of 2.5 bar, the films showed returned to their original resistance value until a threshold pressure value was reached, indicating that the system's morphology was resilient enough to counter the pressure change, in agreement with AFM observation. This resilience results from the hard core/soft corona structure of the micelles and the copolymer chains running through them and connecting them. At 3 bar, the micelles begin to irreversibly deform from spheres to spheroids. This deformation becomes much more pronounced at 3.5 bar (Figure S7) and further at 4 bar when the most of the micelles collapse to irreversibly give a "wormlike" network with uneven large voids, leading to an important porosity change (Figure S8).

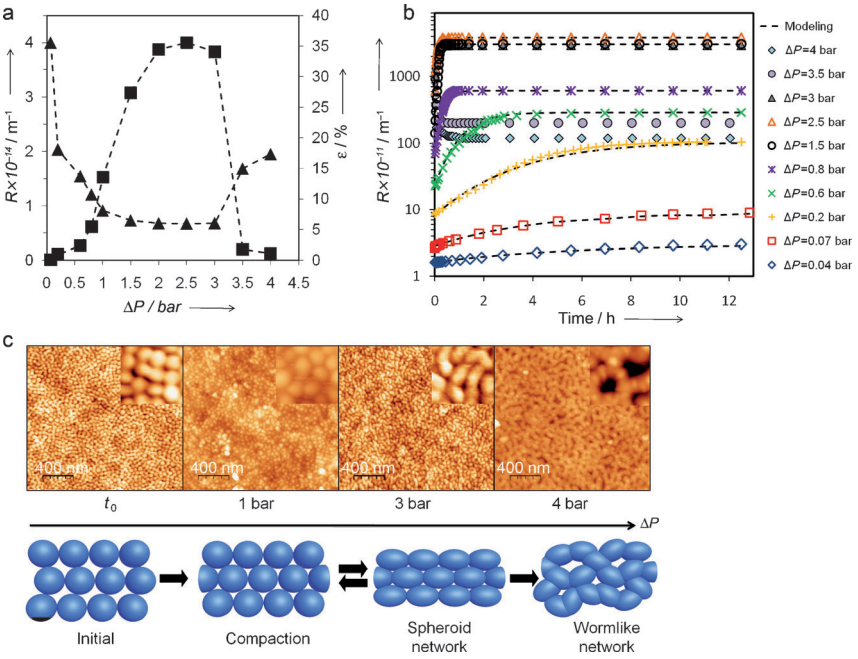

Figure 2. Morphological changes of the nanomaterial under compression: a) Pressure dependence of the water flow resistance R (■) and the calculated porosity ε (▲) after water flux stabilization. b) Excellent correlation of experiment and theory for water flow resistance over time at different pressures. The simulations (dashed lines) combine classical flow laws and a mechanical model of compression (Kelvin–Voigt in series; see the Supporting Information for theoretical calculations). c) AFM images of the top surface of the films before (t_0) and after being subjected for 13 h to different water pressures. Inset: expanded pictures in 250×250 nm. Sketch of the morphological changes from spheres to the wormlike network under compression.

An illustration of this morphological switching is shown in Figure 3, where three successive cycles of increasing and decreasing transmembrane pressure were carried out. The first run, which was stopped below the threshold pressure, shows a strong hysteresis, which can be a result of an increase in the contact surface area between the micelles during compression which thus facilitates PEO interactions. The formation of novel copolymer bridges seems to be realistic since the resistance is maintained while the pressure decreases, attesting to the presence of strong links between the deformed micelles. However, the resistance observed in the first and second runs when the pressure is increased is almost identical, in agreement with reversible formation of the sphere/spheroid morphologies. Interestingly, beyond 3.5 bar, the third run shows almost no hysteresis, which is in agreement with a network of large wormlike pores of very low resistance, which is the usual behavior of classical membranes.

Compared with classical hydrophilic ultrafiltration membranes in which the pore size irreversibly decreases with the applied pressure,[18] these pressure-responsive membranes showing a very sharp change in filtration performances between $\Delta P = 0$ and 4 bar, can operate between reversibly controlled "open" and "closed" states in response to applied

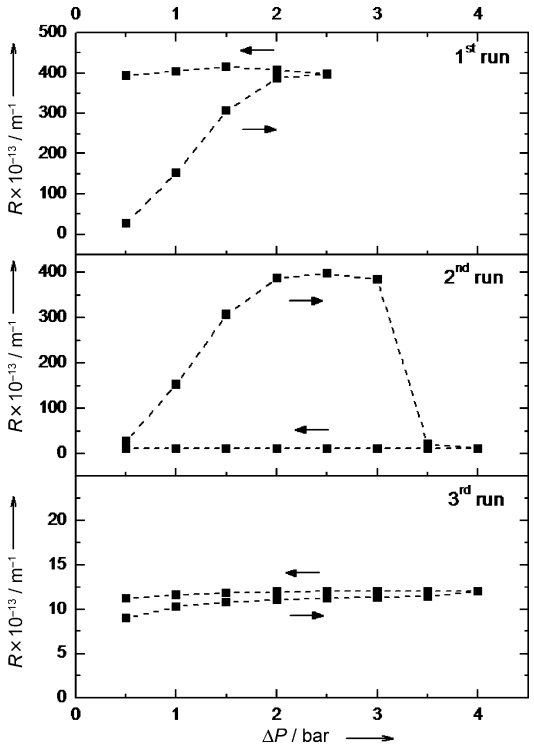

Figure 3. Successive increasing/decreasing cycles of the transmembrane pressure. Each point was obtained after 10 h of equilibrium and after each run the membrane was held for 24 h at atmospheric pressure.

© 2012 Wiley-VCH Verlag GmbH & Co. KGaA, Weinheim

pressures (Figures S9–S12 and Table S2 in the Supporting Information). This assumption is confirmed by permeation of poly(ethylene glycol) (PEG) standards ($M_{n,A}$ = 35000 g mol^{-1}; $M_{n,B}$ = 10000 g mol^{-1}; $M_{n,C}$ = 4600 g mol^{-1}; $M_{n,D}$ = 1450 g mol^{-1}; $M_{n,E}$ = 400 g mol^{-1}) through membranes previously subjected to various water pressures: ΔP = 0.6, 1.5, 2.5, and 4 bar. After treatment with ΔP = 0.6 bar, the retention of all PEGs was found to increase over time as a result of the progressive compression of the micelles (Figure S9). Increasing the pressure to ΔP = 1.5 bar leads to a clear decrease in the pore size; higher retention is observed as only standards D and E could significantly cross the membrane (Figure S10). The retention process is more selective at ΔP = 2.5 bar, where only standard E crosses the membrane (Figure S11). Finally, increasing ΔP to 4 bar leads to a clear increase of the pore size and no retention is observed (Figure S12).

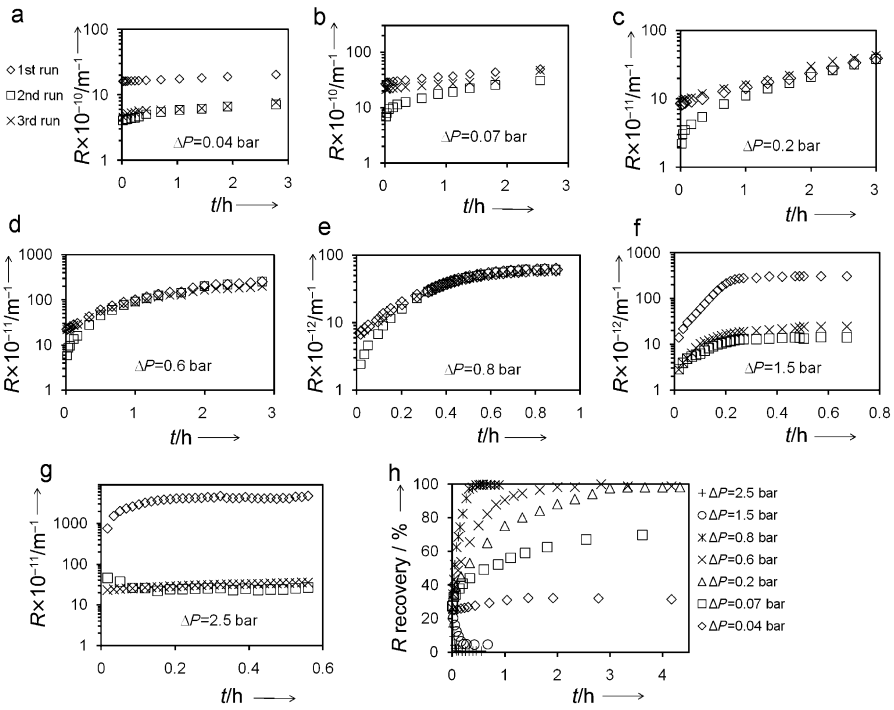

Figure 4. Monitoring the self-healing by recovery of the water flow resistance *R* after the film perforation: *R* recorded over time for the virgin membrane (1st run), during the self-healing stage after a perforation (2nd run), and 24 h after the healing in order to verify the stability (3rd run). a) ΔP = 0.04, b) ΔP = 0.07 c) ΔP = 0.2, d) ΔP = 0.6, e) ΔP = 0.8, f) ΔP = 1.5, g) ΔP = 2.5 bar. h) Pressure dependence of the water flow resistance recovery over time defined by the ratio of the resistance of the virgin membrane to the resistance during the self-healing stage.

It could be presumed that by virtue of the dynamic behavior of the membrane, the self-healing ability of this porous material would be highlighted at the macroscopic level. Currently, self-healing materials are confined specifically to dense systems.[30–34] Imparting self-healing ability to porous materials is noteworthy and though demonstrated theoretically,[35,36] it must still be validated in practice. In the present work, we studied the self-healing ability by damaging the film with a needle leaving a circular perforation of 110 μm in diameter, and then conducting water flow resistance measurements (Figure 4). Given the film thickness of 1.3 μm, the size of the perforation corresponds to almost 85 times the thickness and is a major damage to the material. In general, the *R* value should converge over time to match the first-run curve of the undamaged membrane, if healing has occurred.

As expected, the initial *R* value of the virgin membrane (Figure 4, first run) dramatically decreases immediately after the perforation (Figure 4, second run). A third run was carried out 24 h later to verify the stability of the healing phenomenon (Figure 4, third run). No healing was observed when the perforated films were immersed for one month in water under static conditions; this is in contrast to the films subjected to water flux, establishing the pressure stimulus as the driving force for the self-healing. At very low pressure of 0.04 bar (Figure 4a) very little resistance recovery was measured even after 15 h, while at 1.5 bar and beyond (Figure 4 f,g) the resistance again failed to achieve its original value. These results indicate that there is a pressure range (0.07–0.8 bar) (Figure 4b–e) in which the healing process takes place effectively (Figure 4h). Within this range lowering the pressure increases the time required for the effective healing and vice versa (Figure S13). A perfect match between the first-run curve and third-run curve observed in this range proves the permanent closure of the perforation (see also Figure S14). Figure 5a–e shows SEM pictures of film fragments with a perforation. From images of partially healed and fully healed samples at 0.07 and 0.8 bar, respectively, it can be seen that the perforation is replaced by an uneven surface (Figure 5f). The fragments coming back onto the perforation plane and joining together can also be seen (Figure 5c). No healing is observed for pressures higher than 1.5 bar (Figure 5d), which is in agreement with water flow resistance recovery measurements.

Assuming a healing mechanism that maintains the circular geometry during the closure of the perforation, the healing rate at different pressures can be calculated in terms of repaired surface per unit of time (Figure S15). A maximum healing rate of more than 10 μm^2 s^{-1} has been calculated for a relative pressure of 0.8 bar. All healing rates were found to decrease progressively in the course of healing. A detailed healing mechanism based on a compression gradient across the micelle assembly and the ability to form new block copolymer bridges is proposed in Supporting Information.

In conclusion, self-healing membranes with tunable porosity based on a dynamic set of nanometer-scale block copolymer micelles have been described. The membrane can self-regulate its performance in response to applied water

 © 2012 Wiley-VCH Verlag GmbH & Co. KGaA, Weinheim

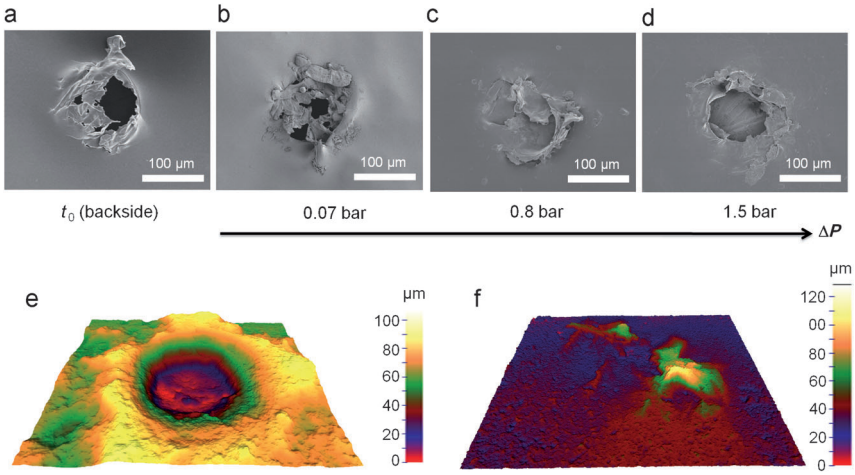

Figure 5. SEM images of the membrane during self-healing: a) Backside image of a perforated film showing downwardly bent film fragments. b) Incomplete healing as a result of the low compression occurring at a pressure of 0.07 bar. c) Complete healing observed after 1 h at 0.8 bar. The scar indicates a random closure of the perforation filled up with overlapping film fragments. d) No healing at high pressure (1.5 bar) making it impossible for the fragments to move back in the perforation plane. e,f) False-color reconstruction of the surface in three dimensions from SEM images at three different angles (90°/80°/70°). e) Perforation in the film causing an elevation of the edges by 40 µm and a depression of film fragments by 60 µm with respect to the plane of the nanomaterial. f) Healed film at 0.8 bar showing a scar above the material plane arising from the random overlapping of the film fragments.

pressure. The tuning of the pore size, and most importantly its functional applicability, is demonstrated by filtration experiments with PEG polymer standards through membranes previously subjected to various water pressures. Despite the low permeabilities,[25,26] (13.4 $L\,h^{-1}\,m^{-2}\,bar^{-1}$ for the spherical-micelle-type membranes and 40 $L\,h^{-1}\,m^{-2}\,bar^{-1}$ for the worm-like-type membranes), the reversible sharp change in the membrane performance controlled by the operating conditions is quite remarkable. Moreover the membrane exhibits the capacity to mend itself at the macroscopic level. Such self-healing films may have a prolonged usable life in a given application without any other external intervention. Block copolymer micelles with adaptive behavior under compression show some formal similarity to functionally complex natural systems for which the communication between different length scales is the central point of the natural selection of functions.[3,37]

Experimental Section

Preparation of membrane films: Membranes were prepared from a 100 $mg\,mL^{-1}$ solution of the triblock copolymer P(Sty_{319}-*co*-AN_{262})-*b*-PEO_{795}-*b*-P(Sty_{319}-*co*-AN_{262}) in DMF/toluene (1:1) (Figure S17).[27] To prevent any external contamination, dried solvents were added through a syringe fitted with a polytetrafluoroethylene (PTFE) filter with a pore diameter of 0.45 µm. The polymer solution was then homogenized under magnetic stirring for 5 days. Small silicon wafers with an area of 25 cm^2 were used for the spin-coating. In order to ensure a clean surface, the wafers were dipped in a 2 wt% solution of a surfactant (RBS35, Chemical products) with sonication. The wafers were then rinsed with ultrapure water and dipped into heptane with sonication. After a second rinse in ultrapure water, the silicon wafers were finally dried under vacuum. The spin-coater was first purged under argon at a pressure of 3 bar for 10 min in order to minimize the presence of water. Several droplets of the polymer solution were passed through a PTFE filter with a pore diameter of 5 µm and deposited onto the silicon wafer which was held by vacuum into the spin coater. The spin coater was then turned on at 2000 rpm for 60 s with a speed ramp of 50 $rpm\,s^{-1}$. Polymer films were then kept under vacuum for 1 day in order to complete the drying process. The coated Si wafers were then dipped into distilled water at 25 °C. After 24 h, membranes were found to be detached from Si wafers and were taken out onto a polyester fabric.

Fluid flow resistance measurements: The block copolymer films (surface area 4.1 cm^2, thickness 1.3 µm) supported on a nonwoven fabric, were enclosed in a dead-end filtration cell and subjected to water pressure. The permeated water was collected in a vessel and the mass gain was recorded as function of time. Fluid flow resistance experiments were conducted at various pressure drops by following the water flux through the micelle assembly over time. The experiments were ended once an equilibrium state was reached.

Perforation experiments**:** The films were first subjected to water pressure to measure the flux evolution as a reference. Then the pressure was relieved and a single perforation was created in the hydrated membrane using a needle having a tip diameter of 110 µm. The needle was put into contact with the assembly membrane/polyester fabric on a silicon wafer to ensure good perforation reproducibility.

Atomic force microscopy: The AFM images were obtained with Dimension 3100-Veeco Instruments. This system of near-field microscopy used for high-resolution imagery was controlled by the Nanoscope IIIA quadrex software. The experiments were all carried out in tapping mode, allowing the capture of topographic images in repulsive mode. The tips used in this study were needles with force modulation provided by Nanosensors (Pointprobe plus–Silicon SPM sensor, with a resonance frequency of about 60 kHz and $K = 2\,N\,m^{-1}$). After water permeation at a given pressure, the membrane was removed along with the nonwoven fabric and let to dry in a closed chamber in the presence of silica gel for 24 h. Once dry, the membrane alone could be manually transferred onto a Si wafer before AFM analysis.

Scanning electron microscopy: The SEM images were obtained using a Hitachi S-4500 instrument operating at spatial resolution of 1.5 nm at 15 kV energy. The samples were analyzed without metallization. For three-dimensional images, images of the samples recorded at different angles were processed using Alicona MeX software. Before SEM analysis the samples were dried in the same way as described above for AFM analysis.

Received: March 1, 2012
Published online: June 13, 2012

Keywords: block copolymers · membranes · self-assembly · self-healing · water filtration

[1] J.-M. Lehn, *Chem. Soc. Rev.* **2007**, *36*, 151 – 160.
[2] M. Barboiu, *Chem. Commun.* **2010**, *46*, 7466 – 7476.
[3] B. Rybtchinski, *ACS Nano* **2011**, *5*, 6791 – 6818.

 © 2012 Wiley-VCH Verlag GmbH & Co. KGaA, Weinheim

[4] R. Nguyen, L. Allouche, E. Buhler, N. Giuseppone, *Angew. Chem.* **2009**, *121*, 1113 – 1116; *Angew. Chem. Int. Ed.* **2009**, *48*, 1093 – 1096.
[5] L. Tauk, A. P. Schröder, G. Decher, N. Giuseppone, *Nat. Chem.* **2009**, *1*, 649 – 654.
[6] S. Mann, *Nat. Mater.* **2009**, *8*, 781 – 792.
[7] B.-S. Kim, I.-K. Park, T. Hoshiba, H.-L. Jiang, Y.-J. Choi, T. Akaike, C.-S. Cho, *Prog. Polym. Sci.* **2011**, *36*, 238 – 268.
[8] H. Kawakami, *J. Artif. Organs* **2008**, *11*, 177 – 181.
[9] P. Kaur, J. T. Hupp, S. T. Nguyen, *ACS Catal.* **2011**, *1*, 819 – 835.
[10] a) E. A. Jackson, M. A. Hillmyer, *ACS Nano* **2010**, *4*, 3548 – 3553; b) E. Krieg, H. Weissman, E. Shirman, E. Shimoni, B. Rybtchinski, *Nat. Nanotechnol.* **2011**, *6*, 141 – 146.
[11] A. Stein, *Adv. Mater.* **2003**, *15*, 763 – 775.
[12] S. D. Bergman, F. Wudl, *J. Mater. Chem.* **2008**, *18*, 41 – 62.
[13] D. Y. Wu, S. Meure, D. Solomon, *Prog. Polym. Sci.* **2008**, *33*, 479 – 522.
[14] J. A. Syrett, C. R. Becer, D. M. Haddleton, *Polym. Chem.* **2010**, *1*, 978 – 987.
[15] M. Ma, R. M. Hill, *Curr. Opin. Colloid Interface Sci.* **2006**, *11*, 193 – 202.
[16] T. Ogawa, B. Ding, Y. Sone, S. Shiratori, *Nanotechnology* **2007**, *18*, 165607.
[17] D. M. He, H. Susanto, M. Ulbricht, *Prog. Polym. Sci.* **2009**, *34*, 62 – 98.
[18] K. M. Persson, V. Gekas, G. Tragardh, *J. Membr. Sci.* **1995**, *100*, 155 – 162.
[19] K. Ebert, D. Fritsch, J. Koll, C. Tjahjawiguna, *J. Membr. Sci.* **2004**, *233*, 71 – 78.
[20] Q. Yang, N. Adrus, F. Tomickiab, M. Ulbricht, *J. Mater. Chem.* **2011**, *21*, 2783 – 2811.
[21] I. Tokarev, S. Minko, *Adv. Mater.* **2009**, *21*, 241 – 247.
[22] T. Schäfer in *Responsive Membranes and Materials* (Eds.: D. Bhattacharyya, R. R. Wickramasinghe, S. Daunert, T. Schäfer), Wiley, Hoboken, **2012**.
[23] O. Ikkala, G. ten Brinke, *Chem. Commun.* **2004**, 2131 – 2137.
[24] S. P. Nunes, R. Sourgrat, B. Hooghan, D. H. Anjum, A. R. Behzad, L. Zhao, N. Pradeep, I. Pinnau, U. Vanio, K. V. Peinemann, *Macromolecules* **2010**, *43*, 8079 – 8085.
[25] S. P. Nunes, A. R. Behzad, B. Hooghan, R. Sourgrat, M. Karunakaran, N. Pradeep, U. Vanio, K. V. Peinemann, *ACS Nano* **2011**, *5*, 3516 – 3522.
[26] K. V. Peinemann, V. Abetz, P. F. W. Simon, *Nat. Mater.* **2007**, *6*, 992 – 996.
[27] D. Quémener, G. Bonniol, T. Phan, D. Gigmes, D. Bertin, A. Deratani, *Macromolecules* **2010**, *43*, 5060 – 5065.
[28] F. C. Giacomelli, I. C. Riegel, C. L. Petzhold, N. P. da Silveira, P. Stepanek, *Langmuir* **2009**, *25*, 731 – 738.
[29] W. Kong, B. Li, Q. Jin, D. Ding, A.-C. Shi, *Langmuir* **2010**, *26*, 4226 – 4232.
[30] S. R. White, N. R. Sottos, P. H. Geubelle, J. S. Moore, M. R. Kessler, S. R. Sriram, E. N. Brown, S. Viswanathan, *Nature* **2001**, *409*, 794 – 797.
[31] P. Cordier, F. Tournilhac, C. Soulie-Ziakovic, L. Leibler, *Nature* **2008**, *451*, 977 – 980.
[32] D. Montarnal, F. Tournilhac, M. Hidalgo, J.-L. Couturier, L. Leibler, *J. Am. Chem. Soc.* **2009**, *131*, 7966 – 7967.
[33] J. W. C. Pang, I. P. Bond, *Compos. Sci. Technol.* **2005**, *65*, 1791 – 1799.
[34] R. S. Trask, I. P. Bond, *Smart Mater. Struct.* **2006**, *15*, 704 – 710.
[35] G. V. Kolmakov, K. Matyjaszewski, A. C. Balazs, *ACS Nano* **2009**, *3*, 885 – 892.
[36] I. G. Salib, G. V. Kolmakov, C. N. Gnegy, K. Matyjaszewski, A. C. Balazs, *Langmuir* **2011**, *27*, 3991 – 4003.
[37] E. Moulin, G. Cormos, N. Giuseppone, *Chem. Soc. Rev.* **2012**, *41*, 1031 – 1049.

 © 2012 Wiley-VCH Verlag GmbH & Co. KGaA, Weinheim